PROTEINS
STRUCTURE ■ FUNCTION ■ BIOINFORMATICS

Solution NMR analysis of the interaction between the actinoporin Sticholysin I and DHPC micelles—Correlation with backbone dynamics

Aracelys López-Castilla,[1,2] Fabiola Pazos,[1] Shirley Schreier,[3] and José Ricardo Pires[2]*

[1] Centro de Estudio de Proteinas, Facultad de Biologia, Universidad de la Habana, Habana, Cuba

[2] Instituto de Bioquímica Médica Leopoldo de Meis, Universidade Federal do Rio de Janeiro, RJ, Brazil

[3] Departamento de Bioquímica, Instituto de Química, Universidade de São Paulo, SP, Brazil

ABSTRACT

Sticholysin I (StI), an actinoporin expressed as a water-soluble protein by the sea anemone *Stichodactyla helianthus*, binds to natural and model membranes, forming oligomeric pores. It is proposed that the first event of a multistep pore formation mechanism consists of the monomeric protein attachment to the lipid bilayer. To date there is no high-resolution structure of the actinoporin pore or other membrane-bound form available. Here we evaluated StI:micelle complexes of variable lipid composition to look for a suitable model for NMR studies. Micelles of pure or mixed lysophospholipids and of dihexanoyl phosphatidylcholine (DHPC) were examined. The StI:DHPC micelle was found to be the best system, yielding a stable sample and good quality spectra. A comprehensive chemical shift perturbation analysis was performed to map the StI membrane recognition site in the presence of DHPC micelles. The region mapped (residues F^{51}, R^{52}, S^{53} in loop 3; F^{107}, D^{108}, Y^{109}, W^{111}, Y^{112}, W^{115} in loop 7; Q^{129}, Y^{132}, D^{134}, M^{135}, Y^{136}, Y^{137}, G^{138} in helix-α2) is in agreement with previously reported data, but additional residues were found to interact, especially residues V^{81}, A^{82}, T^{83}, G^{84} in loop 5, and A^{85}, A^{87} in strand-β5. Backbone dynamics measurements of StI free in solution and bound to micelles highlighted the relevance of protein flexibility for membrane binding and suggested that a conformer selection process may take place during protein–membrane interaction. We conclude that the StI:DHPC micelles system is a suitable model for further characterization of an actinoporin membrane-bound form by solution NMR.

Proteins 2013; 00:000–000.

Key words: actinoporin; protein–lipid interaction; model membrane; toxin; phospholipids.

INTRODUCTION

Actinoporins are a family of pore forming proteins produced by sea anemones.[1,2] These toxins have similar molecular weight (around 20 kDa), no cysteins in their primary sequence, and a remarkable preference for sphingomyelin (SM).[3] Among the most representative members of this family are Sticholysins I (StI) and II (StII), produced by *Stichodactyla helianthus*[4] and Equinatoxin II (EqtII), isolated from *Actinia equine*.[5] The structures of StI, StII, EqtII, and Fragaceatoxin C, another member of the group, have been solved and it was found they share high similarity.[6–10] Their structures consist of a β-sandwich core flanked by two short α-helices (helix-α1 and helix-α2, as in the structure of StI, extracted from the Protein Data Bank, entry 2KS4, displayed with the program molmol (11), Fig. 1).

Actinoporins are synthesized as water-soluble monomers and exhibit a notable capacity to bind to membranes and form oligomeric pores in target cells, provoking lysis. Numerous experimental approaches used to study the pore formation mechanism have permitted to propose a

Additional Supporting Information may be found in the online version of this article.

Abbreviations: CMC, critical micellar concentration; CSP, chemical shift perturbation; DHPC, dihexanoyl phosphatidylcholine; DPC, dodecyl phosphocholine; SM, sphingomyelin; NMR, Nuclear magnetic resonance; PC, phosphatidylcholine; PFG, Pulse field gradient; SAXS, small angle X-ray scattering.

Grant sponsor: CAPES-MES and CNPq-MES cooperation projects, FAPERJ and a Wood-Whelan Research Fellowship (to A.L.C.).

*Correspondence to: José Ricardo Pires, Av. Brigadeiro Trompowiski s/n CCS, Bloco E, sala 10 21941-590 Rio de Janeiro, RJ, Brazil. E-mail: jrmpires@cnrmn.bioqmed.ufrj.br

Received 23 July 2013; Revised 26 October 2013; Accepted 4 November 2013
Published online 12 November 2013 in Wiley Online Library (wileyonlinelibrary.com). DOI: 10.1002/prot.24475

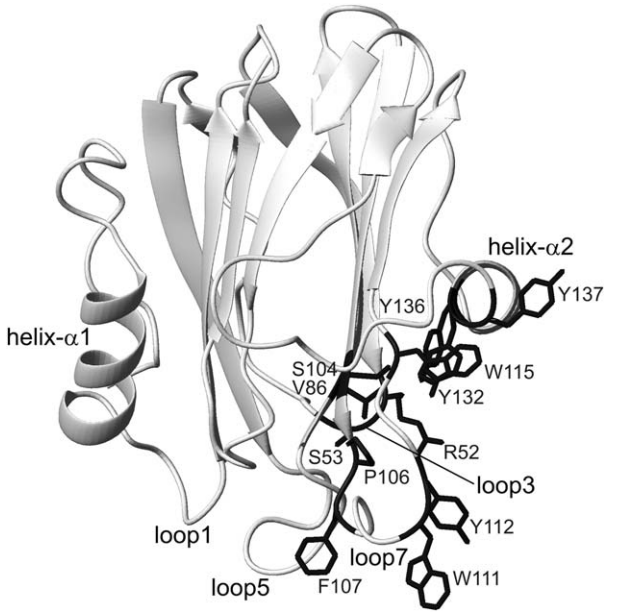

Figure 1

Ribbon representation of StI structure. Side-chains of residues belonging to the cluster of aromatic amino acids and forming part of POC-binding site are shown in black. Helix-α1, helix-α2, and loops at the bottom of the protein structure are labeled. The figure was prepared with MolMol.[11]

model where the first event is the toxin binding to the membrane.[12–14] An exposed cluster of aromatic residues, as well as amino acids involved in the binding of phosphocholine (POC, Fig. 1) seem to be responsible for the initial membrane attachment.[6,15–17] Most of the amino acids comprised in these two regions are located in loops 3 and 7 and in the second α-helix (Fig. 1). Subsequently, the N-terminal segment would detach from the core of the protein and attach to the bilayer surface.[16,18,19]. Finally, several toxin molecules would oligomerize and form the transmembrane pore with the participation of N-terminus region of the protein.[20–23]

Although several studies have been addressed to understand the conformational rearrangements underlying the soluble-to-inserted state transition, the molecular bases driving this process are still poorly understood. One of the main gaps is high-resolution structural and dynamic information about the membrane-bound and pore states of the actinoporins. This is a consequence of technical limitations concerning the research on these protein-membrane systems at the atomic level. In this context, the investigation of bilayer-protein and micelle–protein bound forms at the level of specific residues is of high interest as an appropriate approach to the understanding of the membrane-bound protein conformation. Nuclear magnetic resonance (NMR) spectroscopy is able to provide such kind of information, *for example*, through chemical shift perturbation (CSP) experiments. For actinoporins, two NMR studies of protein–membrane interaction have been published so far. A ^{19}F NMR study of EqtII with all five W residues replaced with 5-fluoro-W allowed distinguishing which amino acids were involved in membrane recognition.[24] More recently, the interaction of StI with dodecyl phosphocholine (DPC) micelles was investigated by solution NMR. In that work, significant broadening of the protein resonances was observed and only the signals of the N-terminal region and the aromatic residues were discussed.[25] Although DPC is one of the most used detergents in solution NMR assays, many other lipids could be employed. Among them, lysophospholipids and short-acyl chain phospholipids are also used.[26–28] These molecules are structurally more similar than DPC to lipids found in cell membranes.

On the other hand, the importance of flexibility for binding to membranes has been reported for several proteins.[29–33] By means of NMR relaxation measurements it has been proposed that proteins could have regions of conformational variability implied in membrane recognition.[34] In the case of actinoporins, the backbone dynamics of two family members, EqtII and StI and two StII mutants, have been investigated for the toxins free in solution,[8,10,35] but the role of protein flexibility for membrane binding has not been studied yet.

To obtain further insight into the structure of membrane-bound forms of actinoporins, we first evaluated different lipid systems for StI:lipid interaction studies by NMR. The lipids tested were lauroyl-lysophosphatidylcholine (12C-lysoPC), palmitoyl-lysophosphatidylcholine (16C-lysoPC), the mixture 12C-lysoPC/lyso-sphingomyelin (lysoSM), and dihexanoyl phosphatidylcholine (DHPC), all of which are capable of forming micelles. Among these systems, DHPC micelles yielded the narrowest lines, suggesting that this is the most promising model for a full characterization of StI structure in a lipid-bound form. Thus, this lipid was used to perform an interaction assay based on CSP studies of StI in the presence of DHPC monomers and micelles. Moreover, with the aim of exploring the relationship between StI dynamic properties and the membrane attachment process, we conducted ^{15}N relaxation measurements of the protein free in solution and in the micelle-bound state.

MATERIALS AND METHODS

DHPC, 12C-lysoPC, 16C-lysoPC and lysoSM were purchased from Avanti Polar Lipids and $^{15}NH_4Cl$ was purchased from Cambridge Isotope Laboratories, Inc. All other reagents were obtained from Sigma-Aldrich Co. (St. Louis, MO).

Expression and purification of StI

Unlabeled and ^{15}N-labeled StI were expressed in *E.coli* Bl21 (DE3) pLysS, following the previously described protocol.[36] For the labeled protein, cells were grown in M9

minimal medium containing 0.5 g/L of $^{15}NH_4Cl$ as the sole nitrogen source. Protein purification was carried out from supernatants of lysed bacteria using ion-exchange chromatography on carboxymethyl cellulose CM52 (Whatman) as previously reported.[36] The protein was concentrated to 0.3–0.5 m*M* in 20 m*M* sodium phosphate buffer (pH 4), 50 m*M* NaCl and 10% (v/v) ^2H_2O.

Preparation of StI:micelles

Lipids were dissolved in chloroform. Appropriate volumes of stock solutions were dried under a stream of nitrogen. The lipid films were left under vacuum for at least 2 hours and micelles were obtained upon addition of protein-containing solutions. Protein and lipid concentrations in the NMR samples were as follows: StI:16C-lysoPC (300 μ*M*: 10 m*M*), StI:12C-lysoPC (600 μ*M*: 20 m*M*), StI:12C-lysoPC/lysoSM (600 μ*M*: 17 m*M*/3 m*M*), StI:DHPC (500 μ*M*: 50 m*M*).

NMR experiments

All NMR spectra were obtained on a Bruker AV-800 spectrometer, equipped with TXI quadruple-resonance (^1H, ^{15}N, ^{13}C, ^2H) probe-head and self-shielded pulsed field gradient in the z direction. Data were acquired and processed by TOPSPIN (v 3.1) (Bruker, Germany). Assignment and analysis of spectra were carried out using SPARKY v 3.1 (T. D. Goddard and D. G. Kneller, University of California, San Francisco). All experiments were recorded at 298 K.

DOSY experiments

Pulse field gradient (PFG) NMR experiments were performed to derive diffusion constants for all St:micelle systems, using the STEbp experiment.[37] The gradient strength was calibrated on the DHPC monomer signals, using the published value of 4.4×10^{-10} m^2 s^{-1} for the self-diffusion coefficient of this molecule.[38] The gradient strength was found to be 38.6 G/cm at the maximum current. Gradient duration d was fixed at 4 ms and the diffusion delay T at 160 ms.

^1H_N, ^{15}N assignment of StI

StI amide signals assignment was based on the data previously reported for this protein (BMRB # 15927).[39] 3D ^{15}N-HSQC TOCSY and ^{15}N-HSQC NOESY were additionally recorded on the protein sample free in solution and in the presence of DHPC micelles to validate the assignment in our experimental conditions.

NMR binding studies

StI lipid binding site was characterized by monitoring chemical shift changes in the ^{15}N-^1H HSQC spectra of 0.3-0.5 m*M* StI as consequence of the stepwise addition of DHPC up to 2.4 m*M*. Under these conditions DHPC was in the monomeric form, since its critical micellar concentration (CMC) is 14 m*M*.[38] For studies with micellar DHPC, a concentration of 50 m*M* lipid was used, which yields a concentration of micelles of approximately 1.3 m*M*, based on an aggregation number (N) of 27[38] and considering that 14 m*M* are in the monomeric form. CSPs of StI amide cross-peaks were calculated using the equation: $\Delta\delta = [\Delta\delta_H{}^2 + (\Delta\delta_N/5)^2]^{1/2}$, where $\Delta\delta_H$ is the observed ^1H chemical shift change and $\Delta\delta_N$ is the observed ^{15}N chemical shift change upon lipid binding.

NMR backbone dynamics

Experiments were performed on ^{15}N labeled StI (500 μ*M*) free in solution and in the presence 50 m*M* DHPC. ^{15}N relaxation times were obtained from a series of 2D ^{15}N-^1H correlated spectra (1024 × 256 data points) with relaxation delays of 0.1, 0.3, 0.6, 1, 2, 4, 6 s for T_1 and 17, 33, 50, 67, 84, 100, 150, 234 ms for T_2, acquired as pseudo-3D datasets in an interleaved manner using the Bruker library pulse programs hsqct1etf3gpsi3d and hsqct2etf3gpsi3d implemented in the program Topspin v3.1. Recycling delays were 1.5 s for T_2 and 8 s for T_1 and the number of scans was set to 8. Cross-peak intensities were fitted as implemented in SPARKY v.3.1 (T. D. Goddard and D. G. Kneller, University of California, San Francisco) to obtain T_1 and T_2 values that were plotted as relaxation rates $R_1 = 1/T_1$ and $R_2 = 1/T_2$. The error in the function fit was considered as the uncertainty in these cases.

Steady-state ^1H-^{15}N Nuclear Overhauser Effects (NOEs) were determined from two 2D ^1H-^{15}N correlation spectra (1024 x 102 data points) as follows: $NOE = I/I_{ref}$, where I is the cross-peak intensity with broadband ^1H pre-saturation and I_{ref} is the intensity without pre-saturation. NOE experiments were acquired in an interleaved manner and splat in two during processing using the standard Bruker library pulse program hsqcnoef3gpsi implemented in the program Topspin v 3.1. Recycling delay was set to 10 s and the number of scans was 32. NOE determinations were performed in duplicate for both free StI and StI:DHPC complex. Average values and standard deviations to the mean were plotted.

Global correlation times (τ_c) for the protein free and bound to the micelles were estimated from the respective R_2/R_1 ratios assuming an isotropic tumbling model, using the program Tensor2.[40] Residues with NOE values below the average and/or undergoing conformational exchange were excluded for the estimation of τ_c.

RESULTS

Evaluation of lipid systems for StI interaction studies

^{15}N-^1H HSQC spectra as well as 2D DOSY were recorded for StI in the presence of micelles consisting of

Table I
PFG-NMR Derived Diffusion Coefficient for Different StI: Micelle Systems

Systems	Ds (m^2/s)
StI + Lyso-PC 16	5.01×10^{-11}
StI + Lyso-PC12/lysoSM micelle	7.76×10^{-11}
StI + Lyso-PC12 micelle	8.91×10^{-11}
StI	1.51×10^{-10}
StI + DHPC micelle	2.00×10^{-10}
DHPC monomers	4.44×10^{-10}

12C-lysoPC, 16C-lysoPC, 12C-lysoPC/lysoSM (85:15), or DHPC to assess the feasibility of protein binding NMR studies using these membrane mimics.

For all lipid systems except DHPC micelles, large molecular complexes were formed as estimated from DOSY derived diffusion coefficients (Ds) (Table I) and extensive line broadening in the HSQC spectra (Supporting Information Figs. S1–S3). Moreover samples were unstable, protein:lipid complexes precipitated in a few hours (probably due to protein denaturation and aggregation, Supporting Information Fig. S3), hampering the acquisition of time demanding NMR experiments. Nevertheless, in the case of a freshly prepared sample of StI bound to 12C-lysoPC micelles (Supporting Information Fig. S1), evaluation of the interaction by CSP is possible, although with limited accuracy.

In contrast, the sample containing StI:DHPC micelles was stable. Larger Ds value and sharper lines in the HSQC spectrum are consistent with somewhat smaller protein–lipid aggregates, appropriate for NMR characterization. Considering these results, all further studies in this paper were performed using DHPC.

Mapping the interaction surface between StI and DHPC

Monomeric DHPC

The interaction of actinoporins with monomeric lipids has been previously investigated.[17,41] However, an NMR study of monomeric lipid titration into an actinoporin sample has not been reported so far, mainly because of the low aqueous solubility and high tendency to aggregate that characterize lipids. The use of NMR experiments for mapping a lipid binding site would permit the identification of all residues involved in lipid recognition. In this research, DHPC was employed to map lipid-interacting residues of StI because it shares the same POC head group of SM; and it has a high CMC (14 m*M*),[38] which allows titration of DHPC monomers into the toxin.

CSP analysis was used to characterize the StI interaction with DHPC molecules. Figure 2 shows the superposed ^{1}H-^{15}N HSQC spectra of StI alone (red contours) and in the presence of DHPC monomers (green contours). Spectral perturbations caused by the addition of DHPC provide evidence for StI–lipid interaction. As shown for the side chain of W^{115} (Fig. 2, inset B), amide signals of most affected residues shift incrementally with respect to the frequencies observed in the free state, indicating a fast exchange on the NMR time scale between StI in the free and DHPC-bound forms.

Figure 3(A) shows ^{15}N, ^{1}H CSP of the StI backbone amides caused by binding of DHPC monomers as a function of residue number. Amino acids with most substantial shifts ($\Delta\delta > 0.038$, *i.e.*, average plus one standard deviation) are highlighted in the StI structure [Fig. 3(B)]. Upon addition of 2.4 m*M* of DHPC, 13 residues showed CSP $\Delta\delta > 0.038$ (G^{84}, A^{85}, F^{107}, D^{108}, Y^{112}, W^{115}, M^{135}, Y^{136}, Y^{137}, G^{138}, N^{151}, M^{162} and the amide side chain of Q^{129}). The most shifted residues were Y^{112} and the side chain of W^{115} in loop 7 and Y^{136}, Y^{137} and G^{138}, located at the end of helix-α2 [Fig. 3(B)].

Micellar DHPC

Micelles are a model membrane widely used to investigate protein-membrane interaction by NMR. Here, we selected DHPC micelles for mapping the StI membrane recognition site.

In the ^{15}N-^{1}H HSQC spectrum of StI (Fig. 2, red contour), larger CSPs were seen in the presence of DHPC micelles (Fig. 2, blue contour) relative to monomers (Fig. 2, green contour). Upon addition of 50 m*M* of DHPC, 22 residues (F^{51}, R^{52}, S^{53}, V^{81}, A^{82}, T^{83}, G^{84}, A^{85}, A^{87}, F^{107}, D^{108}, Y^{109}, W^{111}, Y^{112}, W^{115}, Q^{129}, Y^{132}, D^{134}, M^{135}, Y^{136}, Y^{137}, G^{138}) showed CSP $\Delta\delta > 0.18$ ppm (Fig. 4). Although the regions perturbed in both cases were similar, an additional segment, including residues F^{51} to S^{53}, was only mapped in the presence of micelles (Fig. 4). Residues with largest chemical shift changes were: V^{81}, A^{82}, T^{83}, and G^{84} in loop 5, F^{107}, Y^{112}, and W^{115} in loop 7, and Y^{137} in helix-α2. The region mapped in the presence of micelles clustered mainly one site in StI, which includes loops 3, 5, and 7, and helix-α2 [Fig. 4(B)]. Interestingly, residues at the N-terminal portion showed no significant changes of chemical shift values upon addition of micelles.

Assignment of amide signals in the ^{15}N-HSQC spectrum of StI in its free form was based on the previously reported data for the protein in water[39] and was verified through sequential assignment using conventional 3D ^{15}N-HSQC TOCSY and ^{15}N-HSQC NOESY experiments. The same strategy was used for ^{1}H-^{15}N HSQC spectrum of StI in the presence of DHPC micelles, which allowed unambiguous signals assignment of most amino acids. Nevertheless, five signals in the HSQC spectrum (Fig. 2, indicated by red arrows) could not be assigned by the sequential assignment procedure due to extensive line broadening in the 3D spectra. This group of shifted signals must correspond to residues S^{77}, S^{78}, N^{110}, S^{113}, E^{133}, which are the only amino acids left unassigned in the protein sequence. Indeed they were expected to shift

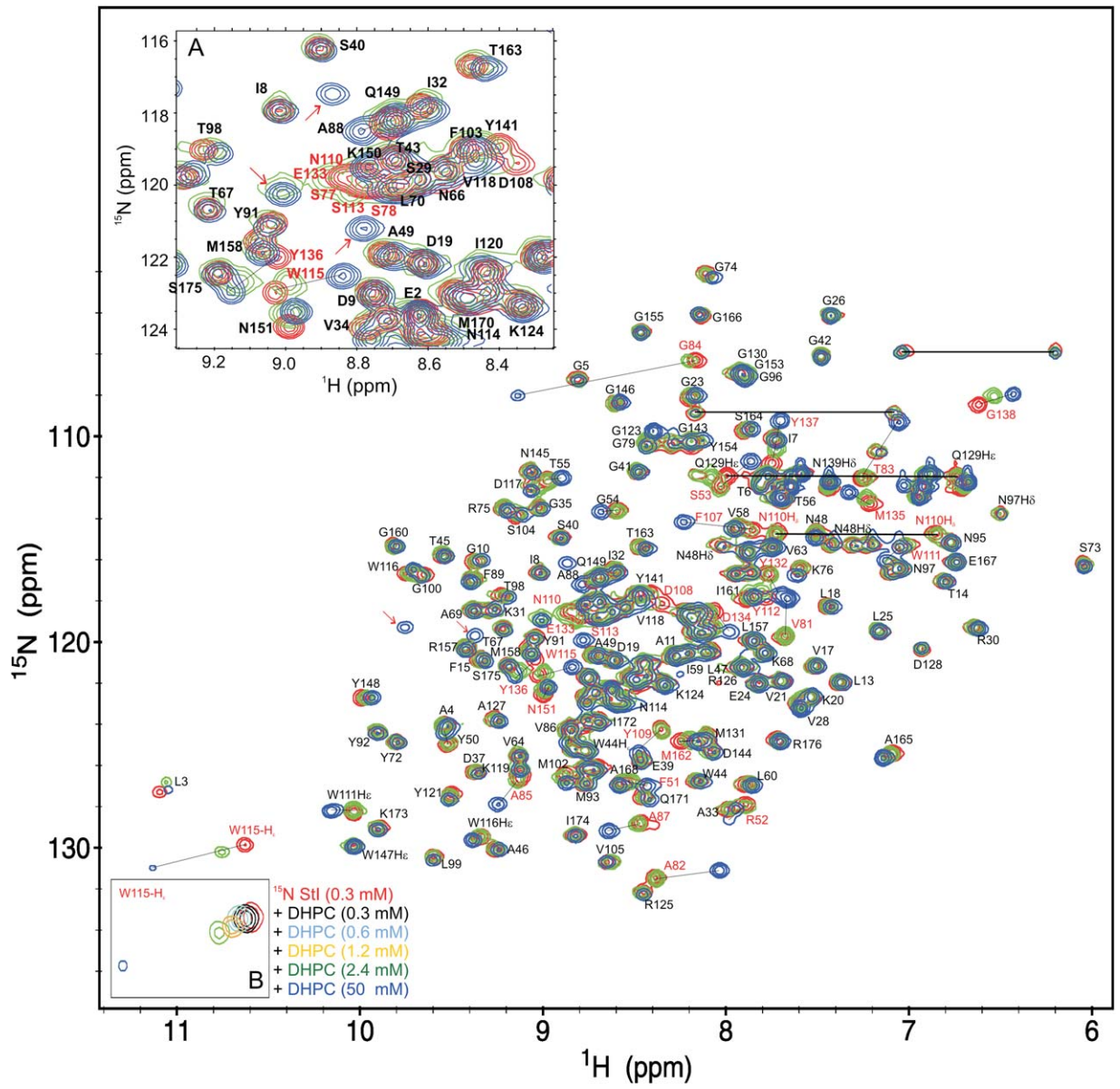

Figure 2

Superposed ^{1}H-^{15}N HSQC spectra of StI (0.3 m*M*) in its free form (red contours) and in presence of 2.4 m*M* of DHPC (green contours) and DHPC micelles (blue contours). Residues exhibiting the greatest chemical shift variations (more than the average plus one standard deviation) are indicated by sequence numbers colored red. Normalized chemical shift changes were calculated according to the equation: $\Delta\delta = [\Delta\delta_H{}^2 + (\Delta\delta_N/5)^2]^{1/2}$. *Inset A*: expansion of an overlapped region of the spectrum. *Inset B*: expansion of W^{115} side chain signal in the presence of increasing amounts of DHPC. Red arrows indicate the five shifted unassigned signals of StI in the presence of DHPC micelles. Concentration of the protein and lipid are inserted and color-coded. The spectra were acquired at 298 K in buffer solution [40 m*M* sodium phosphate buffer (pH 4.5), 50 m*M* NaCl].

based on the other amino acids unambiguously mapped in the presence of micelles.

Dynamic behavior of StI free in solution and complexed with DHPC micelles

NMR measurements of ^{15}N relaxation parameters were employed to characterize the backbone dynamic of StI. Most residues in regular secondary structure exhibited R_1, R_2, and NOEs values close to the average (0.8 s^{-1}, 28.8 s^{-1}, and 0.83, respectively), in contrast to some amino acids in loops (Fig. 5, open circles). The last residues of loop 5 (namely 79–84), as well as V^{28} and V^{34} presented lower R_2 values and decreased NOE, implying higher mobility in ps-ns time scale of these segments. Moreover, residues in loops 7 (Y^{109}, W^{111}) and 9 (N^{139},

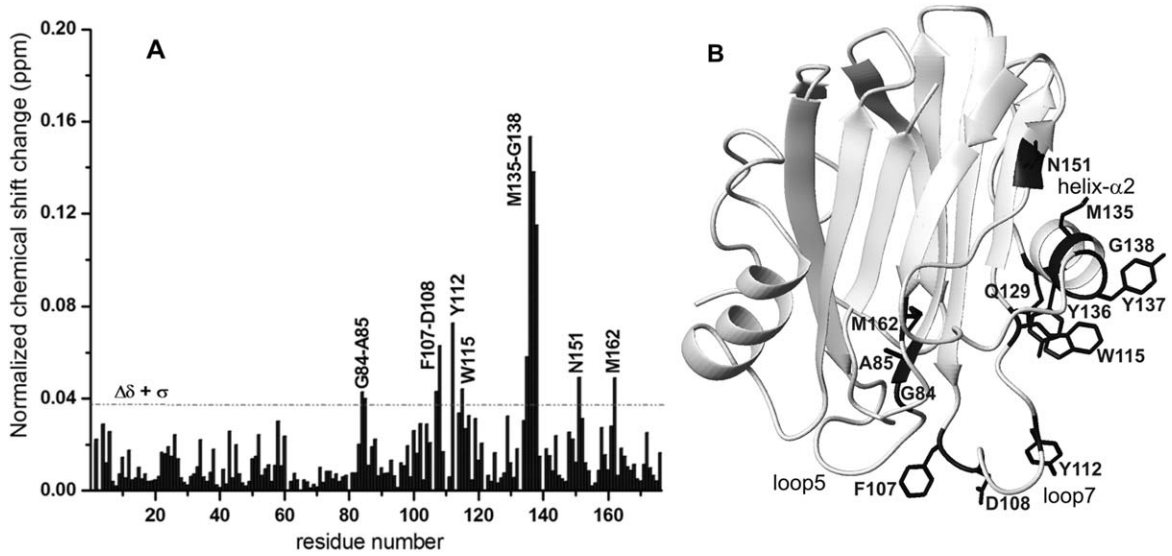

Figure 3

NMR titration of StI with DHPC monomers. (**A**) The histogram shows the CSP of backbone amide signals of StI (0.3 m*M*) in the presence of DHPC monomers (2.4 m*M*) as a function of residues. Missing bars indicate prolines or amide resonances that were not assigned. (**B**) Residues that exhibit significant DHPC-induced resonance perturbation (above the dashed line) are colored black on the StI structure. Helix-α2, loops 5 and 7 are labeled.

Y^{141}, R^{142}) exhibited R_2 values higher than the mean, which points to conformational exchange processes in μs-ms time scale on these regions (Fig. 5, open circles). These dynamics data are in agreement with those previously reported for StI free in solution.[10]

Interestingly, some of the amino acids that showed a different dynamic behavior were also identified as residues that interact with DHPC in the monomeric or micellar form. To investigate the role of StI dynamic properties in membrane binding, we measured the

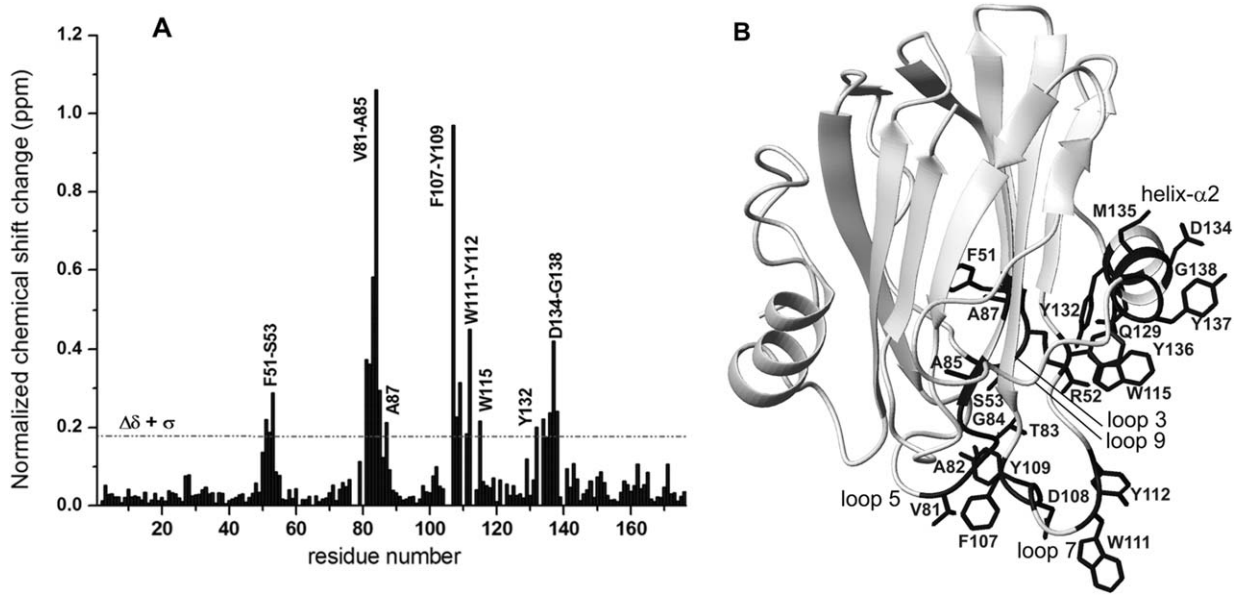

Figure 4

Interaction of StI with DHPC micelles. (**A**) The histogram shows the CSP of backbone amide signals of StI (0.5 m*M*) in the presence of DHPC micelles (50 m*M*) as a function of residue number. Missing bars indicate prolines or amide resonances that were not assigned. (**B**) Residues that display significant chemical shift changes (above the dashed line) are colored black on the StI structure. Helix-α2, loops 3, 5, 7, and 9 are labeled.

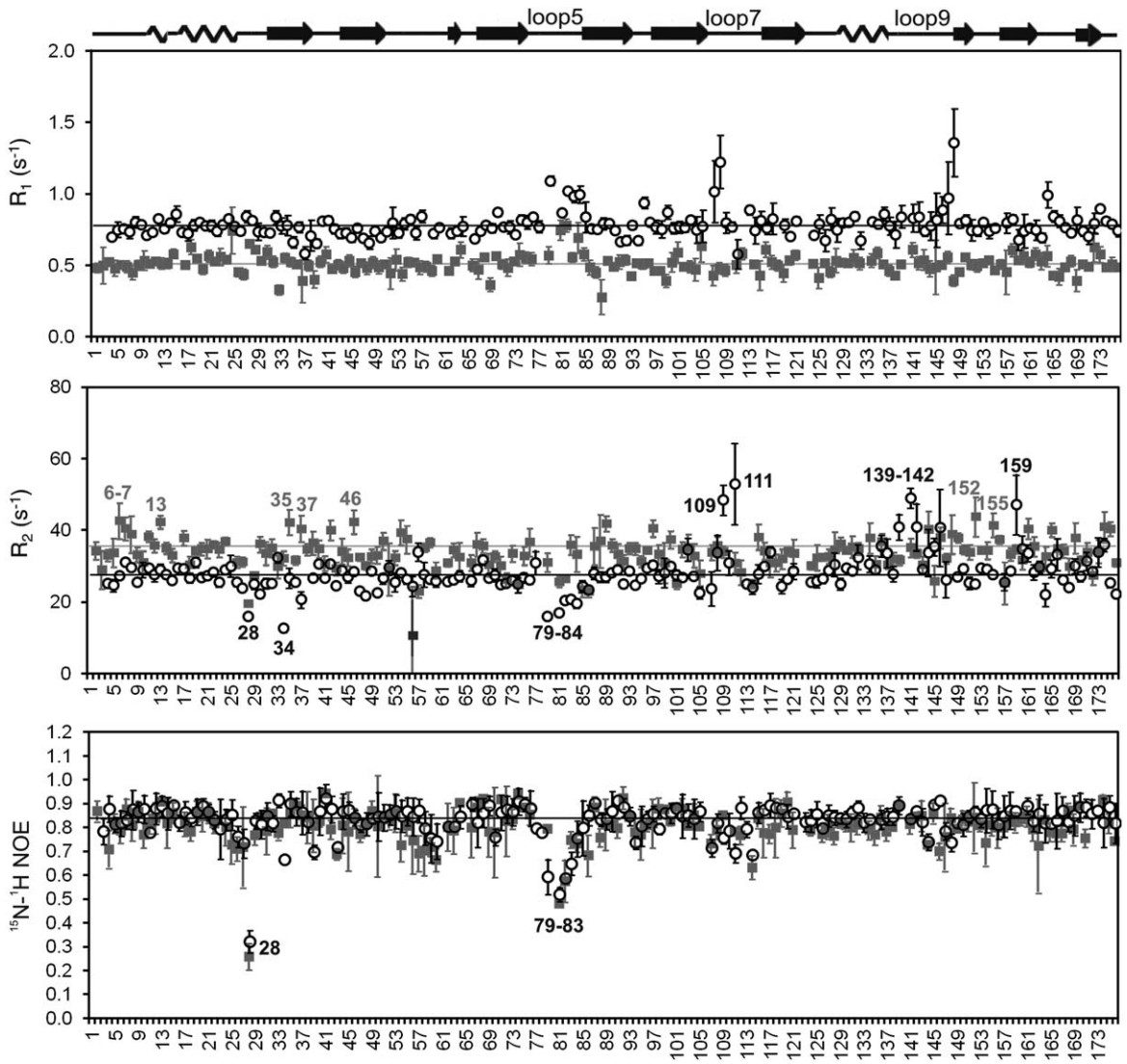

Figure 5

Dynamics from NMR data of StI free in solution 0.5 m*M* (open circles) and in the presence of DHPC micelles (50 m*M*) (gray squares). ^{15}N R_1, ^{15}N R_2 relaxation rates and ^{1}H-^{15}N heteronuclear NOE, as a function of the residue number. The horizontal lines represent the mean values.

relaxation parameters in the presence of DHPC micelles (Fig. 5, gray squares). A global average increase in R_2 (34.2 s^{-1}) and decrease in R_1 (0.5 s^{-1}) values was verified, indicating formation of the protein–micelle complex. That was also corroborated by calculating the global correlation time for StI free in solution (12.7 ns) and bound to micelles (22.4 ns). A decrease in protein local flexibility, mainly for residues in loops 7 and 9, was observed upon lipid binding. In contrast, some residues exhibited a slight increase above the average in R_2 values, such as T^6, I^7, L^{13} at N-terminal region, G^{35} and D^{37} in β-strand 1, A^{46} in β-strand 2 and some amino acids at the C-terminus (L^{152}, G^{155}).

DISCUSSION

StI is expressed as a soluble protein that is able to bind to membranes and to form pores. Although the mechanism of pore formation by actinoporins has been investigated for several years, there are still open questions because of the lack of high-resolution structures of these proteins in the lipid-bound form. Some of these questions are (1) the protein conformational changes caused by the membrane environment, (2) the toxin orientation with respect to the membrane bilayer immediately after attachment and in the pore state, (3) the number of monomers required to form a pore, (4) the pore nature (barrel stave or toroidal) and geometry, (5)

the residues responsible for the oligomerization process and the contacts they establish to stabilize the oligomer.[6,9,24,25]

The binding process has been described as the first step in the mechanism of pore formation.[12–14] Certain residues involved in the bilayer recognition have been identified.[6,15–17] The main strategy used for this purpose has been site-directed mutagenesis together with the evaluation of the mutants binding capacity by different biochemical and biophysical methods.[15–17,21,42] These studies have contributed to define the region(s) in the protein responsible for membrane attachment. In addition, Mancheño *et al.*[6] identified a POC binding site for the actinoporin family. Two NMR studies of the interaction between StI[25] and EqtII[24] with DPC micelles and bicelles, respectively, also provided information about the possible interacting interface and orientation of the protein in the initial bound state. These NMR analyses were incomplete and restricted to a few residues in part because of line broadening and the resulting low resolution NMR spectra obtained with DPC micelles.

Here we performed solution-state NMR experiments, starting with a screening of new lipid systems aiming at improving the NMR data and obtaining a more detailed picture of StI in the membrane-bound form.

Screening for lipid systems

The study of protein–membrane interaction and protein structure bound or inserted in membranes by solution NMR requires the selection of an appropriate membrane mimetic system, with properties resembling the natural membrane. For practical reasons, the system of choice must also result in high quality NMR spectra. Despite some examples of rational choice of the lipids,[43] the effect that different lipids may have on protein structure and quality of spectra is difficult to predict and, in practice, an exhaustive screening of possible lipid systems is necessary.

Thus, we initially evaluated the properties of the four StI-membrane complexes from the NMR point of view. The StI-DHPC micellar system yielded the best quality spectra when compared to the other systems tested; in agreement with the larger Ds value measured for this sample (Table I). The diffusion coefficients for StI:lipid samples were assessed by the lipid signals in DOSY spectra. In the case of StI:DHPC micelles, substantial contributions of DHPC monomers and free DHPC micelles to the observed Ds are expected and explain the larger Ds value measured for this sample (even larger than for StI alone). Indeed, considering the data reported for DHPC (14 m*M* CMC and aggregation number $N = 27$),[38] under our experimental conditions (500 μ*M* StI: 50 m*M* DHPC) we expect a fast exchange equilibrium between about 14 m*M* DHPC in the monomeric form, 22.5 m*M* DHPC in free micellar form, and 13.5 m*M* DHPC in micellar form complexed with StI (assuming a quantitative 1:1 complex formation). For the other lipid systems, the monomeric forms and free micelles are less likely to contribute to the measured diffusion coefficients, in view of the much smaller CMCs and the higher aggregation numbers reported in the literature (for 12C-lysoPC the CMC is 1 m*M* and $N = 55$[44]; for 16C-lysoPC the CMC is 7 μ*M*[45]). The NMR spectra obtained in larger systems (12C-lysoPC, 12C-lysoPC/lysoSM, 16C-lysoPC,) were useless (Supporting information Figs. S1–S3, respectively) because of the broader lines and sample instability. Samples precipitated a few hours after preparation. The spectra shown in Supporting Information Figure S3, suggest a denaturation effect of these micelles on the protein.

DHPC is chemically similar to DPC, the lipid that was used in previous actinoporin NMR studies.[24,25] Both molecules are zwitterionic and have the POC moiety as polar head group but DHPC includes the glycerol moiety and has shorter fatty acid chains (2 × hexanoyl) in comparison to the longer fatty acid chain of DPC (dodecyl). As a result both micelles are geometrically different. In fact, these micelles have been extensively characterized, for instance, using small angle X-ray scattering (SAXS).[46,47] DHPC and DPC micelles are prolate ellipsoids. For the DHPC micelle, average hydrophobic-core axial dimensions (radii) of 22 × 10 × 10 Å (radii ratio 2.2, the nearer to 1, the more spherical is the micelle) and average uniform polar shell thickness of 4 Å were estimated. For DPC micelles, the average hydrophobic-core axial dimensions are 24.5 × 16.2 × 16.2 Å (radii ratio 1.5) and the average uniform polar shell thickness of about 3 Å, aggregation number (N) is approximately 75, and the CMC is 1.5 m*M*. Although these values depend on the experimental conditions and methods used for their determination, they can be employed as an approximation for comparison purposes.

Figure 6 compares the sizes and shapes of DHPC and DPC micelles and StI. Besides the fact that DPC micelles are larger and more spherical than DHPC micelles, differences in other properties—surface curvature, surface area per head group, degree of hydration, compactness of the hydrophobic-core—could account for differences in the interaction between StI and the different micelles tested so far. Concerning line broadening in the NMR spectra, the overall size of the system is an obvious parameter that could result in broader lines. Moreover, the work of Columbus *et al.*[43] suggests that exchange processes could be even more important for line-broadening than system size. In this report, the authors using a peptide containing two coiled-coil transmembrane helices found that sharper lines were obtained when the dominant head to head distance in the micelles matched the hydrophobic extension of the helices. Thinner micelles resulted in structural disruption of the coiled-coil structure to accommodate the hydrophobic helices within the micelle core and thicker micelles

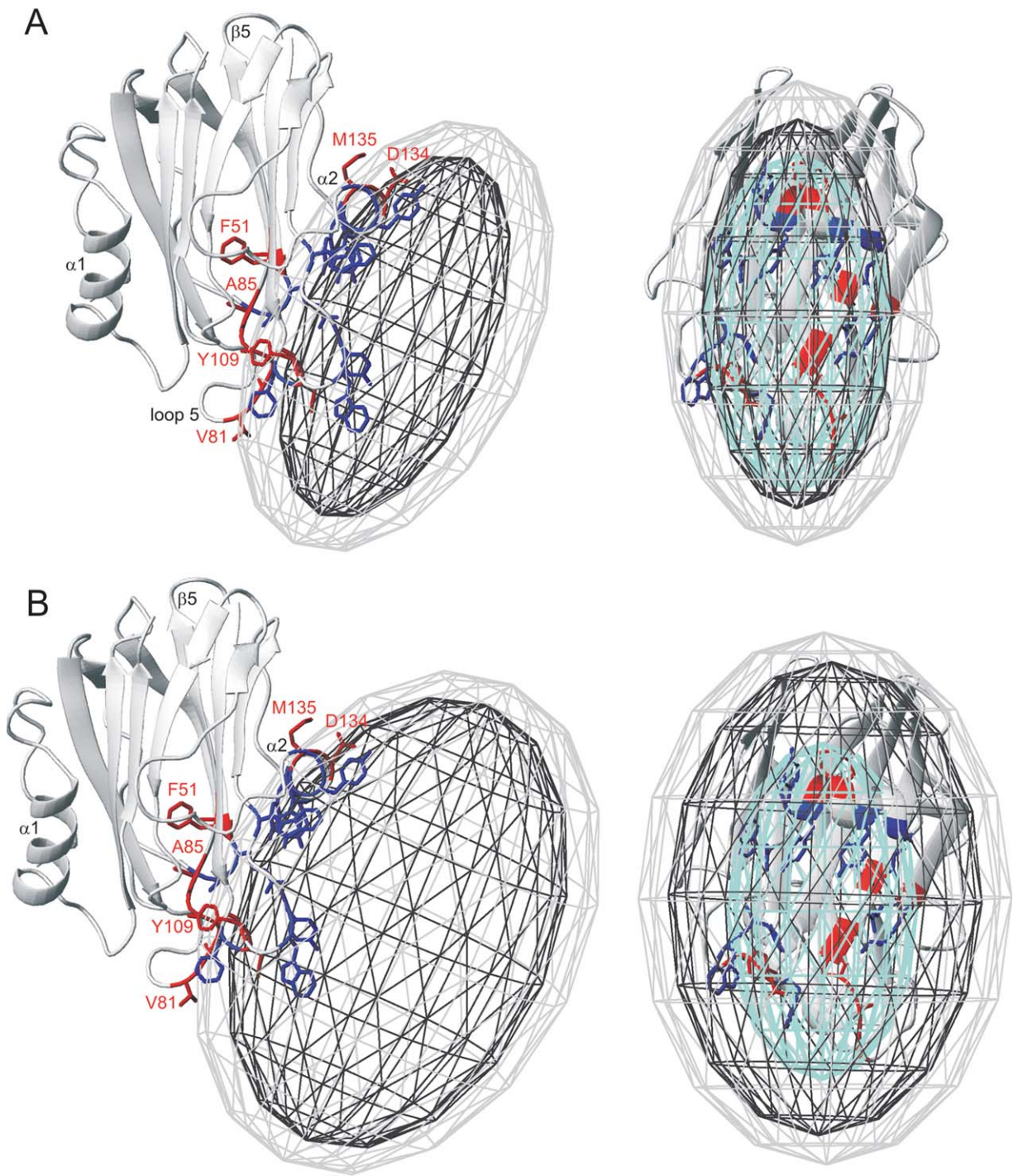

Figure 6

Schematic representation of the interaction between StI and DHPC micelles (**A**) in comparison to DPC micelles (**B**). StI is shown in a ribbon representation and side-chains of residues mapped in the interaction with DHPC are displayed and colored blue (residues in agreement with previous reported data) or red (additional residues mapped in this study). All residues mapped define an almost contiguous region, an ellipsoid colored cyan was added to include all amides mapped. Micelles are represented as gray (polar head groups) and black (hydrophobic core) prolate ellipsoids. Micelles geometry was constructed following SAXS data.[46,47]. Representations at left evidence differences in contacts of residues in loop5 and β5 considering the same insertion of StI in the polar/apolar region of the micelles. Representations at right compare the length and width of the mapped region in StI with the dimensions of the hydrophobic-core of the micelles.

resulted in multiple binding modes exchanging in the μs to ms time scale, both cases leading to low quality NMR spectra. Interestingly, Figure 6 is seen that the extension of the interaction site mapped in StI matches in length and width the hydrophobic-core of the DHPC micelles, yielding few binding alignment possibilities. In contrast, since the DPC hydrophobic-core is much larger than the region mapped in the protein, several exchanging binding modes are possible and could contribute to broader lines. The same reasoning applies to 12C-lysoPC and 16C-lysoPC micelles.

Mapping the DHPC interaction site in StI

The initial approach we used for the protein-membrane interaction study was titration of DHPC monomers into the protein. StI binds DHPC monomers in fast exchange, which is indicative of a weak binding (Fig. 2, insert B). This result is consistent with the fact that actinoporins interact more efficiently with SM than other lipids, including phosphatidylcholine (PC).[17,41] In spite of the fact that SM and PC have the same POC head group, it is known that actinoporins bind more strongly to membranes containing SM[17,41]. Moreover, Eqt II only attaches in an irreversible mode to liposomes containing SM.[17] In contrast, Martinez and co-workers demonstrated that St II is able to bind both SM and PC, although SM in bound in a more efficiently way.[41] The findings presented here reveal that StI, similarly to StII, is capable to interact with PC in a monomeric state. Both StI and StII exhibit higher hemolytic capacity than EqtII.[21,48,49] This peculiar ability of sticholysins of binding one of the most abundant phospholipid of erythrocyte cell membranes, may contribute to the differences in hemolytic activity between sticholysins and EqtII.

The region responsible for StI interaction with DHPC monomers includes 13 residues. Most of them are near (G^{84}, A^{85}, F^{107}, D^{108}, W^{115}, M^{135}, G^{138}) or compose (Y^{112}, Y^{136}, Y^{137}) the POC binding site previously described for St II.[6] Since we used the whole molecule (DHPC) not only the polar head group for studying the lipid-protein interaction, a larger number of amino acids were identified in relation with those reported for POC. In accordance with our results, it was recently proposed that Y^{111} and Y^{136} in StII (corresponding to Y^{112} and Y^{137} in StI, respectively) could form hydrogen bond to the oxygen atom of the SM's phosphate moiety,[50] which is also present in the DHPC molecule.

CSP experiments of StI with DHPC micelles mapped four distinct segments of the StI sequence [Fig. 4(A)]. The first region encloses F^{51}, R^{52}, and S^{53} located in loop 3. All these residues are highly conserved within actinoporin family, suggesting an important role for protein function. In the case of R^{52}, it was previously proposed that its positive charge presumably contributes to stabilize the toxin binding to the POC group.[6] Moreover its substitution by Cys caused a decrease in the lytic activity of the protein, probably due to a less efficient binding to the bilayer.[49] More recently, it was shown that replacement of S^{53} by threonine provoked the decrease of StI membrane binding capacity.[10] The second interacting region encompasses loop 5 (V^{81}, A^{82}, T^{83}, G^{84}) and strand-β5 (A^{85}, A^{87}). These amino acids are highly conserved as well, and form part of a flexible segment in the toxin (Fig. 5, open circles). Loop 5 was the region that underwent the highest CSP in the protein and this result is the first experimental evidence of the contribution of this loop to the actinoporin attachment process.

In addition, binding of DHPC micelles induced significant chemical shift changes for amino acids located in loop 7 (F^{107}, D^{108}, Y^{109}, W^{111}, Y^{112}, W^{115}). F^{107} belongs to the cluster of aromatic residues and its participation in membrane interaction was firstly established by evaluation of EqtII-F^{106}L binding capacity, which was diminished with respect to that of the wild type.[42] Also in agreement with our results, shifts of resonance signals were observed for EqtII W^{112} (W^{111} in StI) and W^{116} (W^{115} in StI) upon addition of DPC micelles and DMPC:DHPC bicelles.[24] Furthermore, the participation of W^{111} and W^{115} in StI-DPC micelle interaction was shown by NMR. As a consequence of micelle binding, W^{111} resonance signal disappeared and W^{115} signal broadened and shifted.[25]

The last region perturbed by DHPC micelles comprises residues in helix-α2 (Y^{132}, D^{134}, M^{135}, Y^{136}, Y^{137}, G^{138}). This result is consistent with the nonameric FraC crystal structure, in which the helix-α2 would lie on the plane of the bilayer in the membrane-bound state.[9] The mapped tyrosines (Y^{132}, Y^{136}, Y^{137}) belong to the cluster of aromatic amino acids and their implication for protein-membrane interaction has also been proved by NMR experiments. Their signals were broadened or disappeared upon interaction of StI with DPC micelles.[25]

In our experimental conditions, resonance signals did not disappear and the assignment process was accomplished for most StI residues in the micelle-bound state. This fact allows us to obtain a comprehensive vision of the interacting region, since chemical shift amide signal of all residues along the protein sequence were checked. This is an advantage in comparison with the two previous solution NMR studies of actinoporin–micelle interaction, where only tryptophans[24] or the N-terminal region and the aromatic residues[25] were discussed. Consequently, the toxin–membrane interaction site was extended by several amino acids, including F^{51} in loop 3, V^{81} to G^{84} in loop 5, A^{85} and A^{87} in β-strand 5, D^{108} and Y^{109} in loop 7, D^{134} and M^{135} in helix-α2.

All amino acids mapped here cluster in an almost contiguous region (Fig. 6). Most residues (Fig. 6, residues with side-chains colored blue) are in agreement with

previous results, others amino acids flank the previous mapped region, like those in loop 5 and β5 and residues D^{108} and Y^{109} in loop 7, D^{134} and M^{135} in helix-α2 (Fig. 6, residues with side-chains colored red). The extended number of residues implicated in the protein–lipid interaction could be a result of the higher resolution and completeness of the NMR data obtained or could be particularly related to the physico-chemical properties of the micellar system used. In any case, the flanking residues indicate that a larger region in StI is in direct contact or undergoing indirect structural changes as a consequence of micelle interaction.

Figure 6 compares the geometries of DHPC and DPC micelles. It is seen that the former, due to the shorter acyl chains, is characterized by smaller axial dimensions leading to a higher curvature. Its polar head group shell is also thicker than that of DPC due to the presence of the glycerol moiety. Moreover, a calculation of the surface area of both particles yields 3942 $Å^2$ and 5925 $Å^2$ for DHPC and DPC micelles, respectively. Taking into account the aggregation numbers for DHPC, $N = 27$[38] and DPC, $N = 75$[47] micelles, one obtains areas of 146 $Å^2$ and 79 $Å^2$ for the molecules in each micelle, respectively, indicating a much looser packing in the head group region and, very likely, also in the acyl chain region in the DHPC micelle, due to the higher curvature. These differences in geometry and molecular packing could allow for a different degree of insertion of StI in the DHPC micelle, leading to a larger number of residues displaying CSPs. Even for the same positioning of StI in the polar/apolar region of the micelles (Fig. 6), a higher number of residues (like the flanking residues mapped here) would be expected to display CSP because of the thicker and less tightly packed polar shell of DHPC.

The interaction of StI with model systems displaying different topographies can be envisioned as the mimicking of different steps in the mechanism of pore formation. Thus, while the binding to planar bilayers would represent the early stages of toxin–membrane interaction, binding to micelles would approximate the protein organization in the toroidal pore. This analogy was proposed for the antimicrobial peptide tritrpticin.[51] Whether the contacts in DPC, DHPC or other micellar system are the more realistic picture for the *in vivo* putative pore cannot be decided on the basis of the present results. Nevertheless, the results suggest the possibility of modulating toxin–membrane contacts, and therefore, the extent of protein penetration, by membrane curvature and molecular packing.

The participation of the N-terminus in the building of actinoporins pore has been clearly established.[12,20,23] No perturbations were observed at the N-terminal segment suggesting that the micelle-bound state studied in this work represents an intermediate state of the pore formation process and ulterior conformational changes may bring this region in closer contact with the lipid–water interface. These findings are in agreement with the model of EqtII and StI, both bound to DPC micelles, in which the N-terminal portion remains in the conformation found in the protein free in solution.[24,25]

Relevance of StI dynamics for membrane binding

Numerous studies have shown that protein dynamics in solution correlates quite well with protein function, especially in the case of movements on μs-ms time scale. The exploration of different conformational spaces by certain segments of a protein, seems to play a relevant role for biological function and, particularly, for protein–protein and membrane–protein interactions.[29–31,33] Until now, there is no report of actinoporin dynamic properties in their bound or inserted state that would allow correlating the flexibility behavior with the membrane interacting ability.

StI dynamics data show two loops undergoing internal motion on μs-ms scale (Fig. 5, labeled open circles). The first one involves residues Y^{109} and W^{111} in loop 7, which is in agreement with the high R_2 values found for the stretch 108–114 in the StI dynamic NMR study recently reported.[10] This loop has also been qualified as a flexible region in the actinoporin crystallographic structures of EqtII[7] and StII.[6] The relevance of local disorder in this region for membrane attachment was suggested from dynamics analysis of the mutant StII Y111N. Perturbation of loop flexibility was related to a loss of mutant lytic capacity.[35] Residues in loop 5 (stretch 79–83) are undergoing fast conformational exchange (in sub-ns time scale) characterized by higher R_1 and smaller R_2 rates and smaller ^1H-^{15}N NOEs than the average. This loop was implicated in the interaction with the micelle, showing strong CSP.

In the presence of DHPC micelles, the dynamic behavior of loop 5 remains unchanged despite of the strong CSP observed, suggesting a loose superficial interaction with the micelle (Fig. 6). On the other hand, the flexibility of Y^{109} and W^{111} decreased and these residues exhibited R_2 values near the average (Fig. 5, labeled grey squares), which suggests a conformational selection process upon protein binding. The other dynamic region exhibiting R_2 values higher than the mean includes amino acids N^{139}, $Y^{141}$and R^{142} in loop 9, which is located near the interacting site. The analysis of StI dynamic behavior in presence of micelles showed a reduction of disorder in this loop as well, suggesting that binding restricts the conformation exchange process. The flexibility of those loops entails the existence of several StI conformers in equilibrium while the protein is in solution. Our dynamics data suggest that membrane recognition involves the selection of one of the pre-existent conformers. Considering that internal motions in those loops are restricted in the bound state, an increase in

flexibility elsewhere in the protein or micelle is expected to compensate the loss of conformational entropy.[52,53] R_2 values higher than the mean were observed for some residues at the N-terminus and at the C-terminal region of the toxin (Fig. 5, grey squares), which could be related to such compensatory changes upon binding. Finally, considering that those two loops are part or are located close to the micelles binding face, the importance of protein plasticity for interacting with membranes is highlighted.

CONCLUSIONS

In summary, this study has permitted to successfully determine the StI membrane recognition site by identifying the residues responsible for StI-DHPC micelles interaction in a comprehensive manner, extending the number of residues involved in the protein–lipid interaction. These results allow a complementary view of the pore formation mechanism, suggesting a deeper insertion or a stronger propagation of changes in the StI structure due to the interaction with the more curved and less tightly packed DHPC micelle. This situation could bear an analogy with biological systems; the interaction with micelles could reflect the StI-membrane interaction at the stage when the protein is attached to the toroidal pore curved surface. Furthermore, we showed that the backbone dynamics of StI is perturbed by binding to the micelle and we propose that this binding may involve a conformational selection process. The good quality of ^{15}N-^{1}H HSQC spectra obtained for this system, together with its stability bring about the possibility of performing future NMR studies, including experiments to solve actinoporins structures in the membrane-bound state.

ACKNOWLEDGMENTS

The authors thank Dr. Aisel Valle for critical reading of the manuscript and helpful suggestions.

REFERENCES

1. Kem WR. Sea anemone toxins: structure and action. In: Hessinger D, Lenhoff H, editors. The biology of nematocysts. New York, NY: Academic Press; 1988. pp 375–405.
2. Macek P. Polypeptide cytolytic toxins from sea anemones (Actiniaria). FEMS Microbiol Immunol 1992;5:121–129.
3. Anderluh G, Macek P. Cytolytic peptide and protein toxins from sea anemones (Anthozoa: Actiniaria). Toxicon 2002;40:111–124.
4. Lanio ME, Morera V, Alvarez C, Tejuca M, Gomez T, Pazos F, Besada V, Martinez D, Huerta V, Padron G, Chavez MA. Purification and characterization of two hemolysins from *Stichodactyla helianthus*. Toxicon 2001;39:187–194.
5. Macek P, Lebez D. Isolation and characterization of three lethal and hemolytic toxins from the sea anemone Actinia equine. Toxicon 1988;26:441–451.
6. Mancheño JM, Martín-Benito J, Martínez-Ripoll M, Gavilanes JG, Hermoso JA. Crystal and electron microscopy structures of sticholysin II actinoporin reveal insights into the mechanism of membrane pore formation. Structure 2003;11:1319–1328.
7. Athanasiadis A, Anderluh G, Macek P, Turk D. Crystal structure of the soluble form of equinatoxin II, a pore-forming toxin from the sea anemone *Actinia equina*. Structure 2001;9:341–346.
8. Hinds MG, Zhang W, Anderluh G, Hansen PE, Norton RS. Solution structure of the eukaryotic pore-forming cytolysin equinatoxin II: implications for pore formation. J Mol Biol 2002;315:1219–1229.
9. Mechaly AE, Bellomio A, Gil-Carton D, Morante K, Valle M, González-Mañas JM, Guerín DM. Structural insights into the oligomerization and architecture of eukaryotic membrane pore-forming toxins. Structure 2011;19:181–191.
10. García-Linares S, Castrillo I, Bruix M, Menéndez M, Alegre-Cebollada J, Martínez-del-Pozo A. Three-dimensional structure of the actinoporin sticholysin I. Influence of long distance effects on protein function. Arch Biochem Biophys 2013;532:39–45.
11. Koradi R, Billeter M, Wüthrich K. MOLMOL: a program for display and analysis of macromolecular structures. J Mol Graphics Modell 1996;14:29–32.
12. Alegre-Cebollada J, Oñaderra M, Gavilanes JG, Martínez-del-Pozo AM. Sea anemone actinoporins: the transition from a folded soluble state to a functionally active membrane-bound oligomeric pore. Curr Protein Pept Sci 2007;8:558–572.
13. Kristan KC, Viero G, Dalla Serra M, Macek P, Anderluh G. Molecular mechanism of pore formation by actinoporins. Toxicon 2009;54:1125–1134.
14. García-Ortega L, Alegre-Cebollada J, García-Linares S, Bruix M, Martínez-del-Pozo A, Gavilanes JG. The behavior of sea anemone actinoporins at the water–membrane interface. Biochim Biophys Acta 2011;1808:2275–2288.
15. Malovrh P, Barlic A, Podlesek Z, Macek P, Menestrina, G Anderluh, G. Structure-function studies of tryptophan mutants of equinatoxin II, a sea anemone pore-forming protein. Biochem J 2000;346:223–232.
16. Hong Q, Gutiérrez-Aguirre I, Barlič A, Marlovrh P, Kristan K, Podlesek Z, Maček P, Turk D, Gonzales-Mañas JM, Lakey JH, Anderluh .G Two step membrane binding by Equinatoxin II, a pore-forming toxin from the sea anemone, involves an exposed aromatic cluster and a flexible helix. J Biol Chem 2002;277:41916–41924.
17. Bakrac B, Gutierrez-Aguirre I, Podlesek Z, Sonnen AF, Gilbert RJ, Macek P, Lakey JH, Anderluh G. Molecular determinants of sphingomyelin specificity of a eukaryotic pore-forming toxin. J Biol Chem 2008;283:18665–18677.
18. Malovrh P, Viero G, Dalla Serra M, Podlesek Z, Lakey HJ, Maček P, Menestrina G, Anderluh G. A novel mechanism of pore-formation: membrane penetration by the N-terminal amphipathic region of equinatoxin. J Biol Chem 2003;278:22678–22685.
19. Gutiérrez-Aguirre I, Barlič A, Podselek Z, Maček P, Anderluh G, Gonzáles-Mañas JM. Membrane insertion of the N-terminal of equinatoxin II, a sea anemone citolytic toxin. Biochem J 2004;384:421–428.
20. Anderluh G, Pungercar J, Krizaj I, Strukelj B, Gubensek F, Maček P. N-terminal truncation mutagenesis of equinatoxin II, a pore-forming protein from the sea anemone *Actinia equina*. Prot Engin 1997;10:751–755.
21. Anderluh G, Barlic A, Podlesek Z, Macek P, Pungercar J, Gubensek F, Zecchini ML, Serra MD, Menestrina G. Cysteine-scanning mutagenesis of an eukaryotic pore-forming toxin from sea anemone: topology in lipid membranes. Eur J Biochem 1999;263:128–136.
22. Kristan K, Podlesek Z, Hojnik V, Gutiérrez-Aguirre I, Guncar G, Turk D, González-Mañas JM, Lakey JH, Macek P, Anderluh G. Pore formation by equinatoxin, a eukaryotic pore-forming toxin, requires a flexible N-terminal region and a stable beta-sandwich. J Biol Chem 2004;279:46509–46517.
23. Kristan K, Viero G, Maček P, Dalla Serra M, Anderluh, G. The equinatoxin N-terminus is transferred across planar lipid membranes and helps to stabilize the transmembrane pore. FEBS J 2007;274:539–550.

24. Anderluh G, Razpotnik A, Podlesek Z, Macek P, Separovic F, Norton RS. Interaction of the eukaryotic pore-forming cytolysin equinatoxin II with model membranes: 19F NMR studies. J Mol Biol 2005;347:27–39.
25. Castrillo I, Araujo NA, Alegre-Cebollada J, Gavilanes JG, Martínez-del-Pozo A, Bruix M. Specific interactions of sticholysin I with model membranes: an NMR study. Proteins 2010;78:1959–1970.
26. Fernandez C, Hilty Ch, Wider G, Wuthrich K. Lipid–protein interactions in DHPC micelles containing the integral membrane protein OmpX investigated by NMR spectroscopy. PNAS 2002;99:13533–13537.
27. Koehler J, Sulistijo ES, Sakakura M, Kim HJ, Ellis CD, Sanders CR. Lysophospholipid micelles sustain the stability and catalytic activity of diacylglycerol kinase in the absence of lipids. Biochemistry 2010; 49:7089–7099.
28. Popovic M, Zlatev V, Hodnik V, Anderluh G, Felli IC, Pongor S, Pintar A. Flexibility of the PDZ-binding motif in the micelle-bound form of Jagged-1 cytoplasmic tail. Biochim Biophys Acta 2012;7: 1706–1716.
29. Frederick KK, Marlow MS, Valentine KG, Wand AJ. Conformational entropy in molecular recognition by proteins. Nature 2007;448:325–329.
30. Henzler-Wildman K, Kern D. Dynamic personalities of proteins. Nature 2007;450:964–972.
31. Mittermaier AK, Kay LE. Observing biological dynamics at atomic resolution using NMR. Trends Biochem Sci 2009, 34:601–611.
32. Medeiros LN, Angeli R, Sarzedas CG, Barreto-Bergter E, Valente AP, Kurtenbach E, Almeida FC. Backbone dynamics of the antifungal Psd1 pea defensin and its correlation with membrane interaction by NMR spectroscopy. Biochim Biophys Acta 2010;1798:105–113.
33. Paula V, Razzera G, Barreto-Bergter E, Almeida FC, Valente AP. Portrayal of complex dynamic properties of sugarcane defensin 5 by NMR: multiple motions associated with membrane interaction. Structure 2011;19:26–36.
34. Valente AP, Miyamoto CA, Almeida FC. Implications of protein conformational diversity for binding and development of new biological active compounds. Curr Med Chem 2006;13:3697–3703.
35. Pardo-Cea MA, Castrillo I, Alegre-Cebollada J, Martínez-del-Pozo Á, Gavilanes JG, Bruix M. Intrinsic local disorder and a network of charge-charge interactions are key to actinoporin membrane disruption and cytotoxicity. FEBS J 2011;278:2080–2089.
36. Pazos F, Valle A, Martínez D, Ramírez A, Calderón L, Pupo A, Tejuca M, Morera V, Campos J, Fando R, Dyszy F, Schreier S, Horjales E, Alvarez C, Lanio ME, Lissi E. Structural and functional characterization of a recombinant sticholysin I (rStI) from the sea anemone *Stichodactyla helianthus*. Toxicon 2006;48:1083–1094.
37. Wu DH, Chen A, Johnson CS. Flow imaging by means of 1D pulsed-field-gradient NMR with application to electroosmotic flow. J Magn Reson A 1995;115:123–126.
38. Chou JJ, Baber JL, Bax A. Characterization of phospholipid mixed micelles by translational diffusion. J Biomol NMR 2004;29:299–308.
39. Castrillo I, Alegre-Cebollada J, del Pozo AM, Gavilanes JG, Santoro J, Bruix M. 1H, 13C, and 15N NMR assignments of the actinoporin Sticholysin I. Biomol NMR Assign 2009;1:5–7.
40. Dosset P, Hus JC, Blackledge M, Marion D. Efficient analysis of macromolecular rotational diffusion from heteronuclear relaxation data. J Biomol NMR 2000;16:23–28.
41. Martínez D, Otero A, Alvarez C, Pazos F, Tejuca M, Lanio ME, Gutiérrez-Aguirre I, Barlic A, Iloro I, Arrondo JL, González-Mañas JM, Lissi E. Effect of sphingomyelin and cholesterol on the interaction of St II with lipidic interfaces. Toxicon 2007;49:68–81.
42. Alegre-Cebollada J, Cunietti M, Herrero-Galán E, Gavilanes JG, Martínez-del-Pozo A. Calorimetric scrutiny of lipid binding by sticholysin II toxin mutants. J Mol Biol 2008;382:920–930.
43. Columbus L, Lipfert J, Jambunathan K, Fox DA, Sim AYL, Doniach S, Lesley SA. Mixing and Matching Detergents for Membrane Protein NMR Structure Determination. J Am Chem Soc 2009;131: 7320–7326.
44. Vitiello G, Ciccarelli D, Ortona O, D'Errico G. Microstructural characterization of lysophosphatidylcholine micellar aggregates: the structural basis for their use as biomembrane mimics. J Colloid Interface Sci 2009;15:827–833.
45. Stafford RE, Fanni T, Dennis EA. Interfacial properties and critical micelle concentration of lysophospholipids. Biochemistry 1989;28: 5113–5120.
46. Oliver RC, Lipfert J, Fox DA, Lo RH, Doniach S, Columbus L. Dependence of Micelle Size and Shape on Detergent Alkyl Chain Length and Head Group. Plos One 2013;8:e62488.
47. Lipfert J, Columbus L, Chu VB, Lesley SA, Doniach S. Size and Shape of Detergent Micelles Determined by Small-Angle X-ray Scattering. J Phys Chem B 2007;111:12427–12438.
48. Alegre-Cebollada J, Lacadena V, Oñaderra M, Mancheño JM, Gavilanes JG, del Pozo AM. Phenotypic selection and characterization of randomly produced non-haemolytic mutants of the toxic sea anemone protein sticholysin II. FEBS Lett 2004;575:14–18.
49. Valle A, López-Castilla A, Pedrera L, Martínez D, Tejuca M, Campos J, Fando R, Lissi E, Alvarez C, Lanio ME, Pazos F, Schreier S. Cys mutants in functional regions of Sticholysin I clarify the participation of these residues in pore formation. Toxicon 2011;58: 8–17.
50. Maula T, Isaksson YJ, García-Linares S, Niinivehmas S, Pentikäinen OT, Kurita M, Yamaguchi S, Yamamoto T, Katsumura S, Gavilanes JG, Martínez-Del-Pozo A, Slotte JP. 2NH and 3OH are crucial structural requirements in sphingomyelin for sticholysin II binding and pore formation in bilayer membranes. Biochim Biophys Acta 2013; 1828:1390–1395.
51. Bozelli JC Jr, Sasahara ET, Pinto MR, Nakaie CR, Schreier S. Effect of head group and curvature on binding of the antimicrobial peptide tritrpticin to lipid membranes. Chem Phys Lipids 2012;165: 365–373.
52. Norton RS. Structures of sea anemone toxins. Toxicon 2009;54: 1075–1088.
53. MacRaild CA, Daranas AH, Bronowska A, Homans, SW. Global changes in local protein dynamics reduce the entropic cost of carbohydrate binding in the arabinose-binding protein. J Mol Biol 2007; 368:822–832.